A limiting current O_2 sensor constituted of $(CeO_2)_{0.95}(Y_2O_3)_{0.05}$ as solid electrolyte layer and $(CeO_2)_{0.75}(ZrO_2)_{0.25}$ as dense diffusion barrier layer

Xiangnan Wang, **Tao Liu** *, **Jingkun Yu**

(School of Metallurgy, Northeastern University, Shenyang 110819, China)

Abstract Using co-precipitation to synthesize $(CeO_2)_{0.95}(Y_2O_3)_{0.05}$ (YDC) and solid reaction method to synthesize $(CeO_2)_{0.75}(ZrO_2)_{0.25}$ (ZDC), and the characterization for both crystal structure and micro-structure of the two materials was conducted with X-ray diffraction (XRD) and scanning electron microscope (SEM) methods. Prepare the YDC and ZDC based limited current O_2 sensor by employing platinum pasting bonding method. Sensing characteristics of the sensor were obtained at different conditions and study on the impact of temperature, O_2 concentration as well as water vapor pressure on the sensing characteristics had been conducted. XRD results show that the phase structure of both YDC and ZDC is cubic phase. SEM results show that both YDC and ZDC layers are dense layers, which are then qualified to be the composition materials of the sensor. This limited current O_2 sensor shows good sensing performance and conforms to the Knudsen model. Log($I_L \cdot T$) depends linearly on 1000/T with R^2 of 0.9904, I_L depends linearly on $x(O_2)$ with R^2 of 0.9726 and sensing characteristics are not affected by $p(H_2O)$.

Keywords Limited current O_2 sensor; YDC solid electrolyte; ZDC dense diffusion barrier; Water vapor pressure

1. Introduction

Electrochemical O_2 sensors are intended for the oxygen concentration detection, therefore are very essential to monitor and control the air fuel ratio (A/F) in the industrial boilers, automotive and metallurgical industries, which contributes a lot to the combustion process optimization, energy savings and emission reductions [1-3]. Concentration potential and limiting current are different principles which make the electrochemical O_2 sensors into two different types [4]. Voltage of the former type of O_2 sensor is correlated to logarithm of the oxygen partial pressure ratio according to Nernst equation, and hence the insensitivity of the voltage to the small changes of the oxygen concentration within a very low range (A/F less than 14.7) [5]. A linear correlation exists between the

* Corresponding author.
E-mail: liut@smm.neu.edu.cn

limiting current of the limiting current O_2 sensor and the O_2 concentration in a certain O_2 concentration range, which indicates high detection sensitivity and therefore the O_2 sensor successfully attracts the public attention [6, 7]. The limiting current O_2 sensor has pore type and dense type according to different types of the diffusion barrier. Pores of the pore type sensor can be blocked by solid particles from the environment without many obstacles. Such disadvantage of the pore type sensor drives the dense type to become hot research focus [8, 9]. Scholars from both domestic China and foreign countries have conducted many researches and studies on limiting current oxygen. Garzon et al. prepared a limiting current O_2 sensors constituted of 8 mol% Y_2O_3 stabilized ZrO_2 (8YSZ) solid electrolyte and $La_{0.84}Sr_{0.16}MnO_3$ (LSM) dense diffusion barrier. The results show that LSM is prone to chemical reaction with YSZ and cracking [10]. Peng et al. prepared a limiting current O_2 sensor with YSZ solid electrolyte and Pt/YSZ mixed materials diffusion barrier. The results show that the limiting current can achieve a plateau when oxygen concentration range is from 0 to 1.8%, but the application of precious metal Pt greatly increases the cost [11]. Therefore, cracks are not easy to appear between solid electrolyte and diffusion barrier, the chemical stability of each other is good at high temperature, and the cost control of the sensor is an important indicator. The oxygen ionic conductivity of Y_2O_3 doped CeO_2 is greatly increased and is a good solid electrolyte with good mechanical properties [12]. Meanwhile, the conductivity of ZrO_2 doped CeO_2 indicates that it has electronic conductivity and can be as a dense diffusion barrier [13, 14]. So YDC and ZDC are assembled to a limiting current O_2 sensor, which have good chemical stability and high electrical conductivity, and may become promising materials for O_2 sensors.

In this paper, the researchers used co-precipitation to synthesize YDC and solid reaction method to synthesize ZDC, and the characterization for both crystal structure and micro-structure of the two materials had been conducted. The YDC and ZDC based limiting current O_2 sensor was prepared by employing platinum pasting bonding method. Study on the impact of temperature, O_2 concentration as well as water vapor pressure on the

sensing characteristics of the O_2 sensor were conducted.

2. **Experimental**

Using co-precipitation to synthesize $(CeO_2)_{0.95}(Y_2O_3)_{0.05}$ (YDC) and solid reaction method to synthesize $(CeO_2)_{0.75}(ZrO_2)_{0.25}$ (ZDC). Directly use all the analytical reagents such as $Ce(NO_3)_3{\cdot}6H_2O$ (purity 99.95%), $Y(NO_3)_3{\cdot}6H_2O$ (purity 99.99%), $NH_3{\cdot}H_2O$ (purity 0.1 M), $Ce_2(CO_3)_3{\cdot}xH_2O$ (purity 99.99%), $ZrOCl_2{\cdot}8H_2O$ (purity 99.9%) and $H_2C_2O_4{\cdot}2H_2O$ (purity 99.99%) without prior purification treatment. Firstly, weigh reagents $Ce(NO_3)_3{\cdot}6H_2O$, $Y(NO_3)_3{\cdot}6H_2O$ and dissolve the reagents in distilled water by intense agitation. Drip reagent $NH_3{\cdot}H_2O$ into nitrate salt solution and continuously stir the mixture until pH reached 9. Wash the obtained precipitate by using distilled water and ethanol, then dry it at 70 ºC, calcine at 800 ºC for 2 h to obtain YDC solid solution powder. Secondly, weigh the stoichiometric reagents $Ce_2(CO_3)_3{\cdot}xH_2O$, $ZrOCl_2{\cdot}8H_2O$ and $H_2C_2O_4{\cdot}2H_2O$ and mill them with agate beads for 96 h. Add 7 wt% Tween 60 into the above reagents at the 48^{th} h. Calcine at 600 ºC for 4 h to obtain ZDC solid solution powder. Analyze the crystal structure of YDC and ZDC powders by using XRD technology (Philips PW3040/60, Netherlands). Press the YDC and ZDC powders and sinter them at 1600 ºC for 6 h in air to obtain sintered bodies for testing. Characterize the micro-structure of sintered bodies YDC and ZDC by SEM equipment (Zeiss, Germany).

Prepare the YDC and ZDC based limiting current O_2 sensor by employing platinum pasting bonding method. Please refer to **Fig. 1** for the structural drawing of the O_2 sensor. Test and record the current-voltage (*I-V*) characteristics of the O_2 sensor by using electrochemical station (LK98BII, China) under different temperatures *T*, oxygen concentrations $x(O_2)$ and water vapor pressure $p(H_2O)$. Adjust the above variable testing conditions by setting the oxygen concentration from low to high, then setting the temperature from high to low and finally setting the water vapor pressure from low to high. Adjust the oxygen concentration by mixing different portions of argon and oxygen to get different Ar/O_2 ratio. Pass dry Ar/O_2 through $LiCl{\cdot}H_2O$ saturated solution to adjust $p(H_2O)$

and $p(H_2O)$ was controlled according to references [15-17]. Total flow rate of Ar/O_2 flows was about 100 ml·min^{-1}.

Fig. 2 demonstrates the *I-V* characteristics testing system [14].

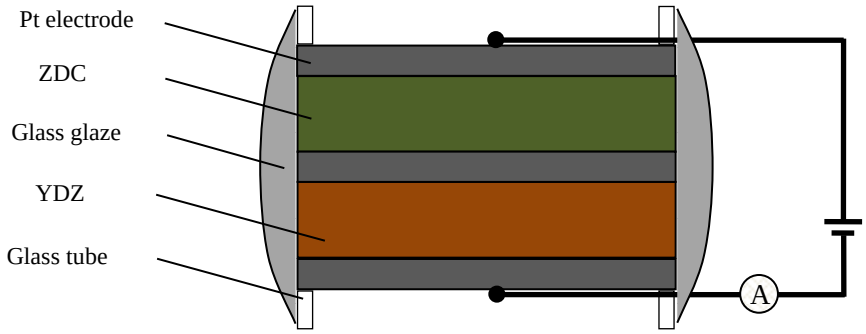

Fig. 1 Structural drawing of the O_2 sensor

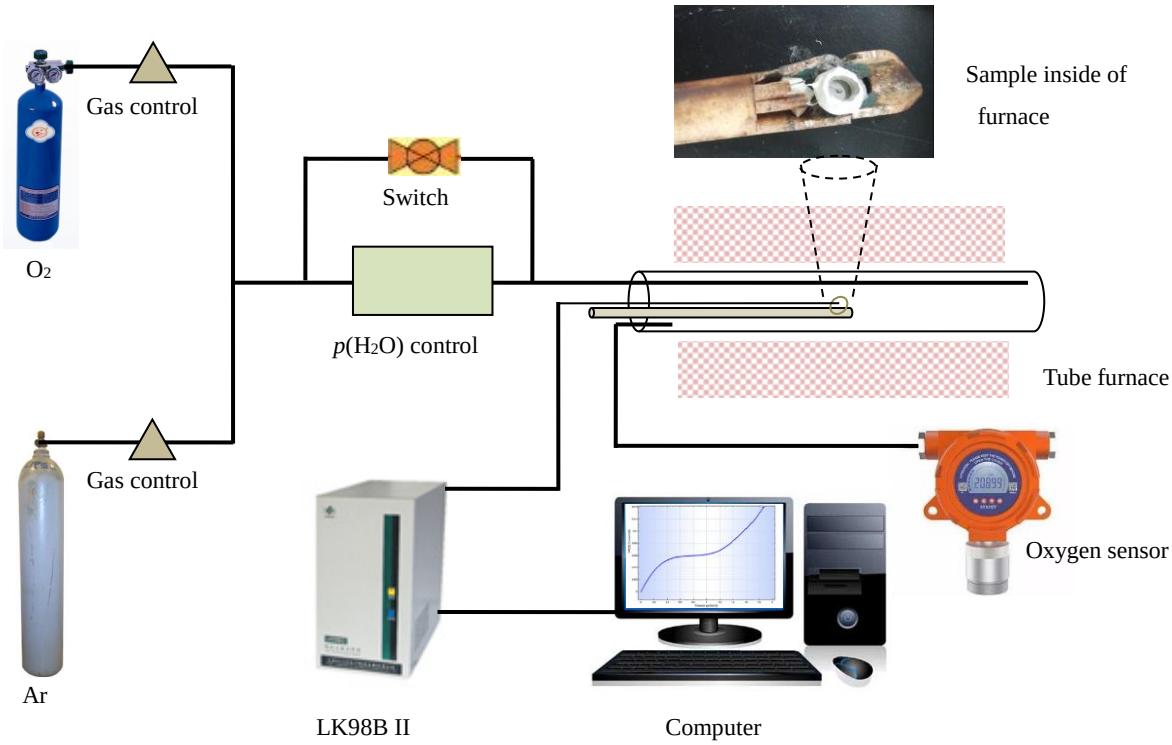

Fig. 2 *I-V* characteristics testing system

3. Results and discussion

3.1 YDC and ZDC

The crystal structure of the YDC and ZDC powders is shown in **Fig. 3 (a)**. It can be seen that YDC and ZDC are cubic phase CeO_2, and a small amount of ZrO_2 diffraction peaks are found in ZDC. The unit cell constants of YDC and ZDC were calculated by GSAS software refinement as shown in **Fig. 3 (b)** and **(c)** [18]. The unit cell constant of YDC is a=b=c of 5.416 and the unit cell volume of 158.841. The unit cell constant of ZDC is a=b=c of 5.404 and the unit cell volume of 157.783. The YDC unit cell constant and unit cell volume are less than YDC due to the Zr ion radius being less than the Y ion radius.

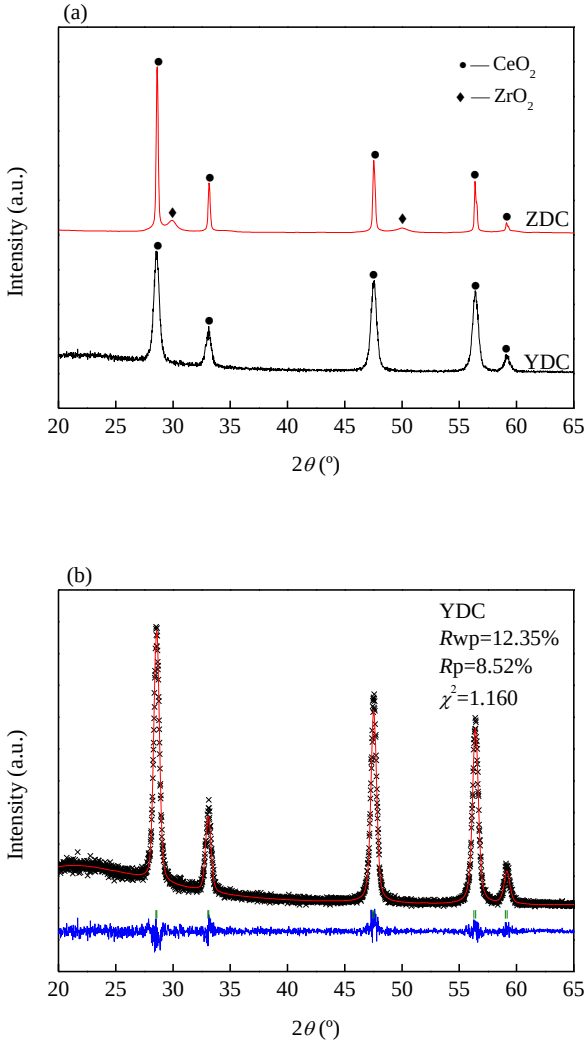

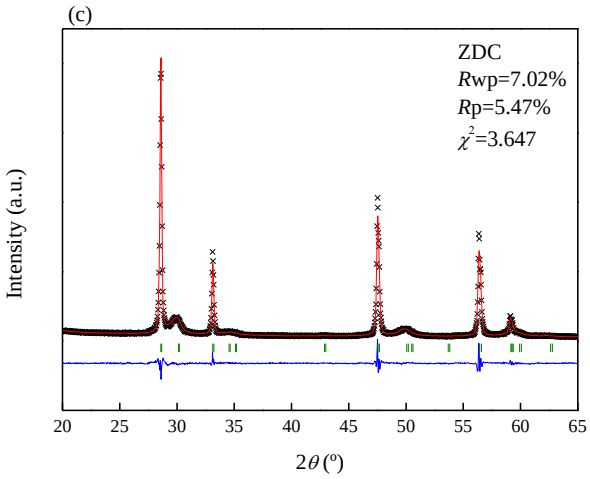

Fig. 3 (a) Crystal structure of the YDC and ZDC, (b, c) unit cell constants of YDC and ZDC

Fig. 4 (a) and **(b)** show the SEM images of YDC and ZDC sintered bodies from the cross-section side, and indicate that the cross-section grain of the sintered body is not obvious and the fracture is transgranular fracture. **Fig. 4 (c)** and **(d)** illustrate the elemental distributions of YDC and ZDC powders, which also clearly show that the molar ratios of Y to Ce and Zr to Ce are substantially comply with the stoichiometric ratios of YDC and ZDC solid solutions, respectively.

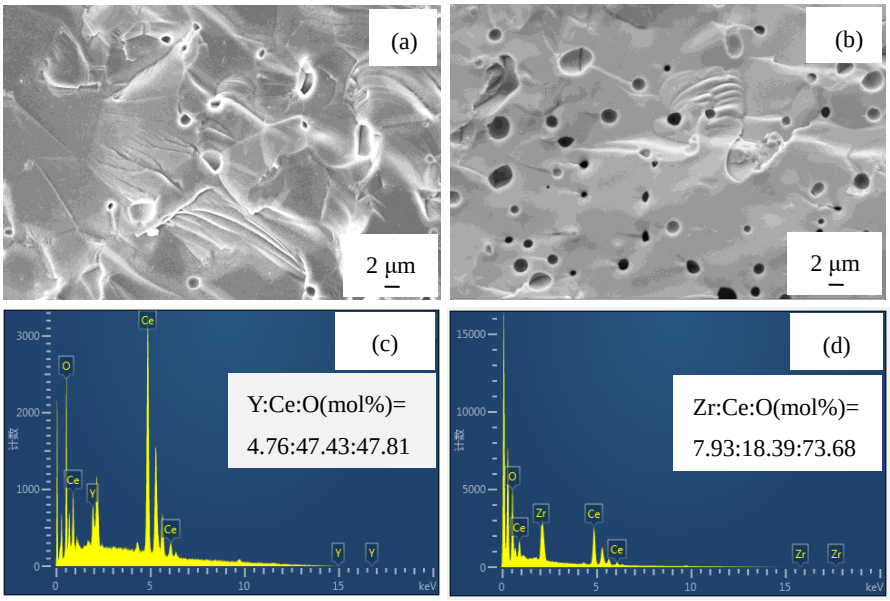

Fig. 4 (a, b) SEM images of YDC and ZDC sintered bodies, (c, d) elemental distributions of YDC and ZDC

The ionic conductivity of YDC and ionic, electronic conductivity of ZDC are shown in **Fig. 5 [**12**].** The electrical conductivities and temperature satisfy the Arrhenius law and the fittings have good fitting degree R^2 of 0.9978 for ionic conductivity of YDC, 0.9992 for ionic conductivity of ZDC and 0.9848 for electronic conductivity of ZDC, respectively. The electrical conductivities of YDC and ZDC meet the requirements of solid electrolyte layer and dense diffusion barrier layer of the limiting current O_2 sensor, respectively.

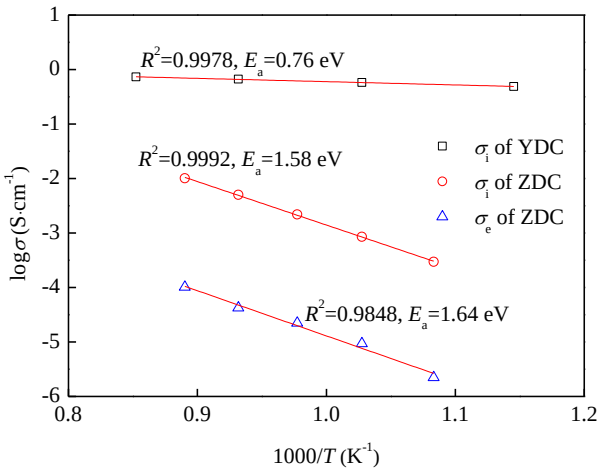

Fig. 5 Ionic conductivity of YDC and ionic, electronic conductivity of ZDC

3.2 *I-V* and *T*

Measure the *I-V* characteristic of the YDC and ZDC based O_2 sensor within the temperature range of 710-830 °C and control the O_2 concentration at 2.50% to obtain the *I-V* characteristic curves as demonstrated in **Fig. 6**, according to which, we can conclude that the curves mainly contains two areas, namely the ohmic area and the limiting current plateau area. In area I, with the increase of applied voltage, the output current increases linearly, owing to the ohmic behavior of YDC layer of the sensor [19]. The ohmic slope has a certain relationship with the electrical conductivity of the solid electrolyte, and their change tendencies are the same. Meanwhile, electrical conductivity of the solid electrolyte increases or decreases just as temperature does, therefore, ohmic slope will also change toward the same direction as temperature does. In area II, slope of the *I-V* curve changes compared to that in area I, and the current in this area reaches plateau or close to plateau. Average current in this area is the limiting current value of the O_2 sensor. Without a diffusion barrier, output current in area II will increase as the voltage increases, and the curve slope will be the same as that in area I. However, with a diffusion

barrier, oxygen will be blocked, and hence the reduced volume of oxygen that pass through the solid electrolyte layer, which then generates a new *I-V* slope. Voltage at junction of the two areas is the initial voltage of O_2 sensor, and normally the lower the initial voltage value is, the more sensitive the sensor is. There is a negative correlation between initial voltage and temperature, meaning initial voltage will decrease as temperature increases, because conductivity of ZDC dense diffusion barrier will increase as temperature increases.

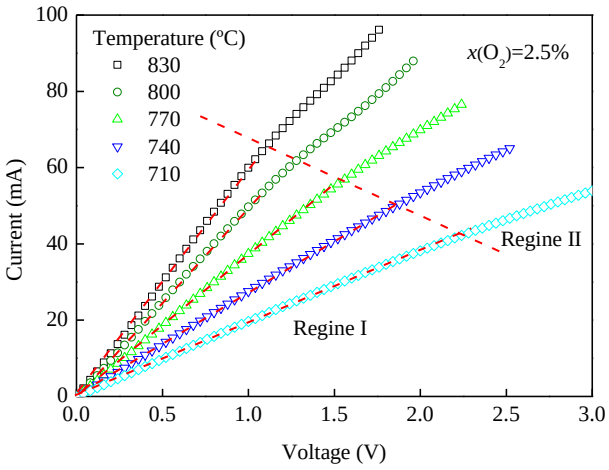

Fig. 6 *I-V* characteristic curves at different temperature

3.3 *I-V* and $x(O_2)$

Fig. 7 demonstrates the *I-V* characteristic curves of the YDC and ZDC based O_2 sensor with oxygen concentration from 0.4% to 1.9% and temperature at 800 °C. During the research, oxygen is adsorbed to the outside surface of the dense diffusion barrier, then, by absorbing two electrons at the (ZDC/Pt/air) triple phase boundaries at high temperatures, the absorbed oxygen becomes oxygen ions. Since the diffusion barrier is a mixed ionic-electronic conductor, the potential applied to both sides thereof is 0, and under the driving of the oxygen pressure difference, oxygen ions are transported from the surface of ZDC layer to the ZDC/YDC interfaces. Similarly, oxygen ions become oxygen molecules by losing electrons and the oxygen molecules will be released at the triple phase boundaries. Migration rate of oxygen ions from ZDC/YDC interfaces to YDC outside surfaces is affected by the voltage applied to the YDC layer. Oxygen pumping rate increases as the applied voltage increases, and the limiting current plateau can be reached when the voltage increases to a certain level and oxygen pumping

rate from YDC layer is limited by oxygen diffusion rate from ZDC layer. When the pumping rate of the YDC solid electrolyte is limited by the oxygen diffusion rate of the ZDC dense diffusion barrier and the voltage increases to a certain value, the limiting current plateau is obtained. Initial voltage is positively related to oxygen concentration, which is consistent with phenomenon of other studies [20, 21].

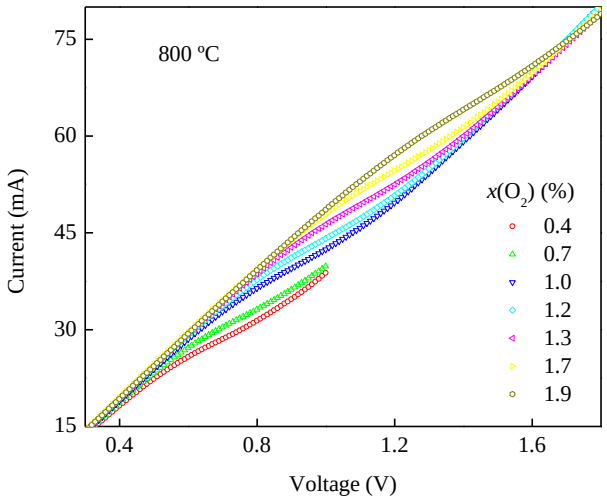

Fig. 7 *I-V* characteristic curves in different $x(O_2)$

Fig. 8 demonstrates the linear correlation between the limiting current and the oxygen concentration at the temperature of 800 °C, and the linear correlation coefficient R^2 is 0.9726. Refer to reference [2] for Knudsen diffusion correlation theory, which is the same as this correlation.

$$I_L = \frac{4FD_K SP}{RTL} \cdot x(O_2) \quad (1)$$

where D_K is the oxygen diffusion coefficient, P the partial pressure difference between electrodes, T the temperature, F the Faraday constant, R the gas constant, S the total cross-sectional area and L the length of diffusion path, respectively.

Solid state theory of solid ion diffusion mode, diffusion coefficient (D_T) and temperature (T) is as follows:

$$D_T = D_O \cdot \exp\left(-\frac{\varepsilon}{k_B T}\right) \quad (2)$$

where D_O is the constant of the frequency factor, ε the activation energy for the diffusion process and k_B the

Boltzmann constant, respectively.

Equation (3) is obtained by simultaneous equations (1) and (2):

$$I_L = \frac{4FD_OSP}{RLT} \cdot x(O_2) \cdot \exp(-\varepsilon/k_BT) \quad (3)$$

Assuming the oxygen concentration is stable, then:

$$a = \frac{4FD_OSP}{RL} x(O_2) \quad (4)$$

Equation (5) is obtained by introducing equation (4) into equation (3):

$$I_L = a \cdot \frac{1}{T} \cdot \exp(-\varepsilon/k_BT) \quad (5)$$

Equation (6) is obtained by solving the logarithm of equation (5):

$$\log I_L = A - \log T - \frac{\varepsilon}{k_BT} \quad (6)$$

and then,

$$B = -\frac{\varepsilon}{k_B} \quad (7)$$

So get equation (8):

$$\log I_L = A - \log T + B \cdot \frac{1}{T} \quad (8)$$

Equation (9) is obtained by sorting out:

$$\log (I_L \cdot T) = A + B \cdot \frac{1}{T} \quad (9)$$

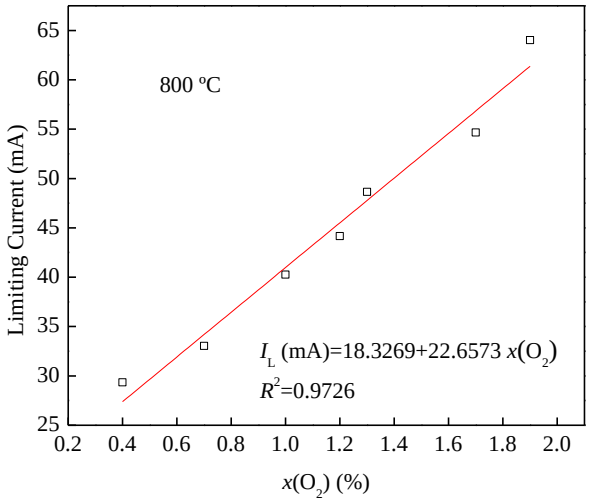

Fig. 8 Limiting current and the oxygen concentration at the temperature of 800 ℃

Fig. 9 demonstrates the linear relationship between $\log(I_L \cdot T)$ and 1000/T in $x(O_2)$ of 2.5% according to equation (9)**,** and the linear correlation coefficient R^2 is 0.9904. This relationship meets the Knudsen diffusion model.

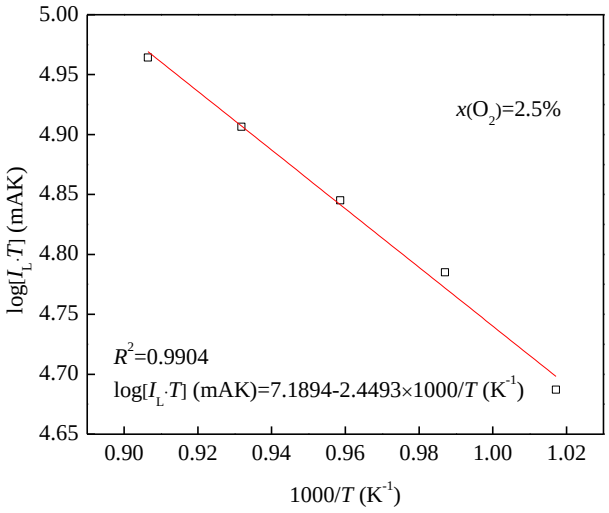

Fig. 9 The $\log(I_L \cdot T)$ and 1000/T in $x(O_2)$ of 2.5%

3.4 *I-V* and $p(H_2O)$

Fig. 10 demonstrates the effect of $p(H_2O)$ on *I-V* characteristic curves in oxygen concentration of 1.2% and at temperature of 800 °C. As can be seen that the sensing characteristics of the O_2 sensor obtained are almost coincide under different $p(H_2O)$, indicating that the $p(H_2O)$ does not have significant effect on the *I-V* characteristics within the test range. Some studies on the influence of $p(H_2O)$ on the limiting current sensor show that the porous type sensor is affected by $p(H_2O)$, while the dense type sensor is not affected [14, 22, 23]. The O_2 sensor has excellent selectivity to O_2, which is an excellent indicator of the sensor.

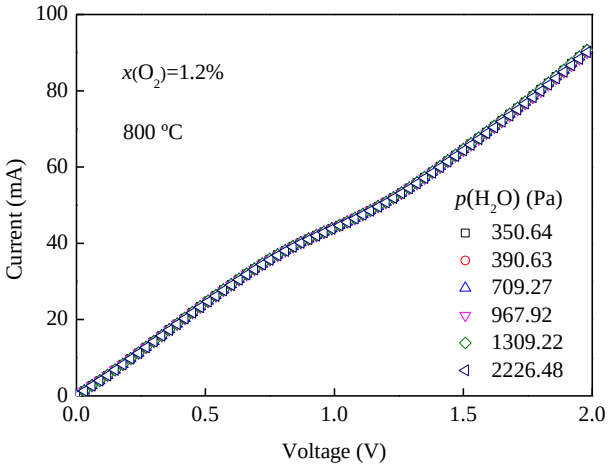

Fig. 10 *I-V* characteristic curves and $p(H_2O)$ in oxygen concentration of 1.2% and at temperature of 800 °C

Conclusions

Using co-precipitation to synthesize YDC and solid reaction method to synthesize ZDC. Prepare a YDC and ZDC based limiting current O_2 sensor by platinum pasting bonding method. XRD results show that YDC and ZDC belong to cubic phase structure. SEM results show that the sintered bodies are dense and conform to the materials for limiting current O_2 sensor. $\mathrm{Log}(I_L \cdot T)$ depends linearly on $1000/T$ with R^2 of 0.9904, I_L depends linearly on $x(O_2)$ with R^2 of 0.9726 and sensing characteristics are not affected by $p(H_2O)$, which indicating that the O_2 sensor has excellent sensing characteristics and conforms to Knudsen model.

Acknowledgement

This work is financially supported by the National Natural Science Foundation of China (51374055) and the Fundamental Research Funds for the Central Universities of China (N172506007).

References

[1] T. Liu, X.F. Zhang, L. Yuan, J.K. Yu, A review of high-temperature electrochemical sensors based on stabilized zirconia, Solid State Ion. 283 (2015) 91–102.

[2] J.X. Han, F. Zhou, J.X. Bao, X.J. Wang, X.W. Song, A high performance limiting current oxygen sensor with $Ce_{0.8}Sm_{0.2}O_{1.9}$ electrolyte and $La_{0.8}Sr_{0.2}Co_{0.8}Fe_{0.2}O_3$ diffusion barrier, Electrochim. Acta 108 (2013) 763–768.

[3] T. Liu, X.F. Zhang, X.N. Wang, J.K. Yu, L. Li, A review of zirconia-based solid electrolytes, Ionics 22 (2016) 2249–2262.

[4] X.N. Wang, T. Liu, J.K. Yu, Y.C. Mo, M.Y. Yi, J.Y. Li, L. Li, Preparation and electrical property of $CaZr_{0.7}M_{0.3}O_3$ (M=Fe, Cr and Co) dense diffusion barrier for application in limiting current oxygen sensor, Sens. Actuator B-Chem. 266 (2018) 455–462.

[5] A.D. Brailsford, E.M. Logothetis, Selected aspects of gas sensing, Sens. Actuator B-Chem. 52 (1998) 195–203.

[6] T. Liu, X. Gao, B.G. He, J.K. Yu, A limiting current oxygen sensor based on LSGM as solid electrolyte and LSGMN (N = Fe, Co) as dense diffusion barrier, J. Mater. Eng. Perform. 25 (2016) 2943–2950.

[7] X.F. Zhang, T. Liu, J.K. Yu, X. Gao, H.B. Jin, X.N. Wang, C. Wang, A limiting current oxygen sensor with $La_{0.8}Sr_{0.2}(Ga_{0.8}Mg_{0.2})_{1-x}Fe_xO_{3-\delta}$ dense diffusion barrier, J. Solid State Electrochem. 21 (2017) 1323–1328.

[8] T. Liu, X.N. Wang, X.F. Zhang, X. Gao, L. Li, J.K. Yu, X.T. Yin, A limiting current oxygen sensor prepared by a co-pressing and co-sintering technique, Sens. Actuator B-Chem. 277 (2018) 216–223.

[9] Y.C. Mo, T. Liu, C. Wang, A limiting current oxygen sensor based on $(La_{0.4}Ce_{0.6}O_{2-\delta})_{0.96}(FeO_{1.5})_{0.04}$ as dense diffusion barrier, Ceram. Int. 45 (2019) 8319–8324.

[10] F. Garzon, I. Raistrick, E. Brosha, R. Houlton, B.W. Chung, Dense diffusion barrier limiting current oxygen sensors, Sens. Actuator B-Chem. 50 (1998) 125–130.

[11] Peng Z Y, Liu M L, Balko E, A new type of amperometric oxygen sensor based on a mixed-conducting composite membrane, Sens. Actuator B-Chem. 72(2001) 35–40.

[12] C.Z. Wang, Solid electrolytes and chemical sensors, Metallurgical Industry Press. 100.

[13] X.N. Wang, T. Liu, C. Wang, J.K. Yu, L. Li, Crystal structure, microstructure, thermal expansion and electrical conductivity of CeO_2-ZrO_2 solid solution, Adv. Appl. Ceram. 116 (2017) 477–481.

[14] X.N. Wang, T. Liu, J.K. Yu, L. Li, X.F. Zhang, A new application of $Ce_xZr_{1-x}O_2$ as dense diffusion barrier in limiting current oxygen sensor, Sens. Actuator B-Chem. 285 (2019) 391–397.

[15] N.A. Gokcen, Vapor pressure of water above saturated lithium chloride solution, J. Am. Chem. Soc. 73 (1951) 3789–3790.

[16] T.W. Chung, C.M. Luo, Vapor pressures of the aqueous desiccants, J. Chem. Eng. Data 44 (1999) 1024–1027.

[17] P. Kolár, H. Nakata, A. Tsuboi, P. Wang, A. Anderko, Measurement and modeling of vapor-liquid equilibria at high salt concentrations, Fluid Phase Equilib. 228-229 (2005) 493–497.

[18] B.H. Toby, EXPGUI, a graphical user interface for GSAS, J. Appl. Cryst. 34 (2001) 210–213.

[19] T. Usui, A. Asada, M. Nakazawa, H. Osanai, Gas polarographic oxygen sensor using an oxygen / zirconia electrolyte, J. Electrochem. Soc. 136 (1989) 534–542.

[20] X. Gao, T. Liu, J.K. Yu, L. Li, Limiting current oxygen sensor based on $La_{0.8}Sr_{0.2}Ga_{0.8}Mg_{0.2}O_{3-\delta}$ as both dense diffusion barrier and solid electrolyte, Ceram. Int. 43 (2017) 6329–6332.

[21] X. Gao, T. Liu, X.F. Zhang, B.G. He, J.K. Yu, Properties of limiting current oxygen sensor with $La_{0.8}Sr_{0.2}Ga_{0.8}Mg_{0.2}O_{3-\delta}$ solid electrolyte and $La_{0.8}Sr_{0.2}(Ga_{0.8}Mg_{0.2})_{1-x}Cr_xO_{3-\delta}$ dense diffusion barrier, Solid State Ion. 304 (2017) 135–144.

[22] C.M. Mari, G. Rabotti, Humidity determination by solid state limiting current sensor, Solid State Ion. 124 (1999) 309–315.

[23] S. Akasaka, Thin film YSZ-based limiting current-type oxygen and humidity sensor on thermally oxidized silicon substrates, Sens. Actuator B-Chem. 236 (2016) 499–505.